High Energy Processes in Solar Flares

Reuven Ramaty* and Natalie Mandzhavidze†

*NASA/GSFC, Greenbelt, MD 20771
†NASA/GSFC and USRA, Greenbelt MD 20771

Abstract.
We review the highlights of the high energy processes in solar flares. Particle acceleration is an essential ingredient of the flare energy release process. Among all cosmic high energy sources, flares are unique in that both the accelerated particle and the radiations that they produce are observed. In this paper we emphasize the radiations, gyrosynchrotron emission, bremsstrahlung and gamma ray lines. These provide information on flare models, magnetic fields, energy content in the accelerated particles and abundances. The abundances are not only critical for constraining the acceleration mechanisms, but also provide unique information on solar atmospheric dynamics and mixing, solar wind acceleration, and Galactic chemical evolution.

INTRODUCTION AND OVERVIEW

Major cosmic explosion are essentially always accompanied by particle acceleration. In the solar system, solar flares are the most powerful particle accelerators, capable of accelerating ions to at least a GeV and electrons to at least hundreds of MeV. Evidence for particle acceleration at the Sun comes from both direct particle observations in interplanetary space (e.g. [1]), and electromagnetic radiations which can only be produced by accelerated particle interactions in the solar atmosphere, specifically radio emission (e.g. [2]), hard X-rays (e.g. [3]) and gamma rays, (e.g. [4]). Such interactions also produce neutrons which are detected in space and near Earth (e.g. [5]). The ability to observe both the accelerated particles themselves and the radiations that they produce is a unique feature of solar flare acceleration. For other cosmic sites, the presence of accelerated particles can only be inferred from the radiations they produce.

Unlike some cosmic explosions (e.g. gamma-ray bursts) whose luminosities peak in the hard X-ray and gamma-ray bands, the radiative output of solar flares is maximal in a band ranging from optical to EUV wavelengths (e.g. see figure 1 in [6]). Nevertheless, there are compelling arguments, based on the impulsiveness [7] and energetics of the hard X-ray and gamma-ray emissions, that flares are fundamentally high-energy phenomena. The energy contents in flare accelerated electrons of energies $\gtrsim 20$ keV, derived from the X-ray data [8], and ions of energies

$\gtrsim$ 1MeV/nucleon, obtained [9,4] from gamma ray data [10], can exceed about 10^{32} erg, comparable to the total radiative output of the flare. How the flare releases this energy, most likely stored in the coronal magnetic fields, and how it rapidly accelerates electrons and ions with such high efficiency, is not yet completely understood.

Studies of solar energetic particle (SEP) observed in interplanetary space have shown that these SEP events can be classified as impulsive and gradual [11–14]. Impulsive events, for which the associated soft X-ray emission is of relatively short duration, have large electron-to-proton ratios (e/p), large ^{3}He/^{4}He, large heavy ion (particularly Fe) to C or O ratios, and charged states corresponding to temperatures which significantly exceed the (1–2)$\times 10^6$K coronal temperature. Gradual events, for which the soft X-rays last longer, exhibit smaller e/p, and have heavy ion abundances, ^{3}He/^{4}He, and charged states which are consistent with coronal abundances and temperatures. It is reasonable to associate the above two classes of SEP events with different acceleration mechanisms. Because of the strong association with coronal mass ejections (CMEs), particles in gradual events are probably accelerated out of coronal gas by the CME driven shock (e.g. [15]). On average, $\sim 10^{15}$ g of material is ejected per CME with speeds ranging from $\sim$100 to $\sim$2000 km/sec (see [16]). The maximal kinetic energy of a CME is thus comparable to the energy released in large flares. Some of the CMEs travel fast enough in the corona to drive collisionless shock waves which can accelerate particles. On the other hand, particle acceleration in impulsive events is probably due to gyroresonant interactions with plasma waves (see [17,18]).

In this paper on high energy processes in solar flares, we focus on the radiations that reveal the existence of the accelerated particles at the Sun. We first discuss the bremsstrahlung and gyrosynchrotron radiation and next the gamma ray line emission.

RADIATIONS PRODUCED BY ACCELERATED PARTICLES IN SOLAR FLARES

The radiations produced by the particles accelerated in solar flares are observed at high energies, as hard X-rays and gamma rays, and at very low energies, as radio waves extending in frequency up to the millimeter region. The bulk of the hard X-rays is bremsstrahlung produced by accelerated electrons. This bremsstrahlung extends from about 20 keV, where it merges with thermal bremsstrahlung produced by hot flare plasma, up to energies of hundreds of MeV [19]. In the energy region from about 0.3 to 8 MeV there are nuclear lines superimposed on the bremsstrahlung continuum [7]. Above about 50 MeV, in some flares there is emission resulting from the decay of pions, which are produced in the interactions of the highest energy protons and α particles with the ambient solar atmosphere (e.g. [20]).

Bremsstrahlung and Gyrosynchrotron Radiation

In the hard X-ray region, the central issue is that of the energy content in the sub-relativistic electrons. Within the well accepted electron bremsstrahlung paradigm, the fact that the energy lost by the electrons to bremsstrahlung is only a small fraction of the energy lost to Coulomb collisions, leads to an energy content in the electrons which is comparable to the total radiative output of the flare. That the hard X-rays are indeed bremsstrahlung is strongly supported by the fact that other X-ray producing mechanisms, specifically inverse Compton scattering, cannot account for the observations, mainly because of the low target photon densities. On the other hand, the question of whether the bremsstrahlung is driven by accelerated electrons or ions has often been raised (e.g. [21]). Most recently, it has been shown that at least some hard X-ray production could be due to the electrons in neutralized ion beams [22]. But the near simultaneous brightening of loop footpoints in hard X rays [23] is strong evidence that for these flares relativistic electron driven bremsstrahlung is the dominant process.

At hard X-ray energies, above about 100 keV and well into the gamma ray region, the solar flare continuum is definitely electron driven bremsstrahlung. Perhaps the best evidence for this is the strong correlation between the high energy continuum and the microwave/millimeter emission. The top panel of Figure 1 shows the time profiles of the gamma ray emission above 1 MeV and the 80 GHz millimeter emission observed near the impulsive peak of the 1991 June 4 flare [24,25]. A series of 6 very large (X-class) solar flares occurred in June 1991 and gamma ray emission was observed from all of them. These very large flares also produced very intense millimeter emission. The millimeter flux observed from the 1991 June 4 flare, shown in Figure 1, is in fact the largest ever observed [26]. The gamma ray emission observed from this flare was in fact so intense that it saturated all four instruments on the Compton Gamma Ray Observatory (CGRO), except the Charged Particle Detector (CPD) which is part of the BATSE instrument on CGRO. The CPD had no energy resolution, which is the reason that the gamma ray time profile shown in Figure 1 is the integral flux above 1 MeV. The middle panel in Figure 1 shows the measured ratio between the millimeter and gamma ray fluxes. The dip in the ratio is due to the delay (a few seconds) of the gamma ray emission relative to the millimeter flux.

A relatively simple model [25] that can account for these observations is one in which the millimeter emission is thin target gyrosynchrotron radiation produced in the upper parts of magnetized coronal loops, while the gamma ray emission is thick target bremsstrahlung produced at the loop footpoints. Thin and thick target refer to the behavior of the electrons, thin target meaning that the electrons precipitate from the upper, gyrosynchrotron production region before they lose any appreciable amount of energy into the thick target footpoint regions where they slow down and stop as they produce the bremsstrahlung. Because of the high frequency considered (80 GHz), the gyrosynchrotron source is optically thin. The lower panel in Figure 1 shows the calculated ratio of the 80GHz gyrosynchrotron emission to the $>$1 MeV bremsstrahlung as a function of the power law index S of the accelerated electrons, for several values of the magnetic field in the upper, thin target region. Another parameter is the electron trapping time $\tau = 15$sec in this region, which follows from

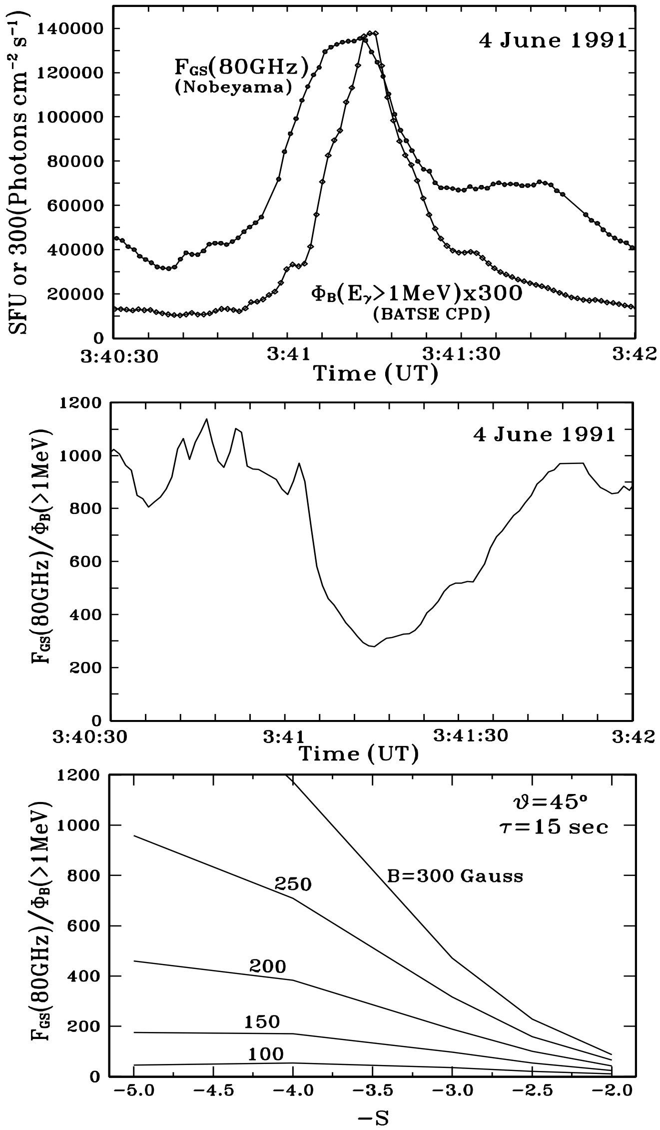

FIGURE 1. Top panel: gamma ray and millimeter wave time profile near the impulsive peak of the flare which produced the largest millimeter wave emission ever observed; middle panel: the ratio of the millimeter and gamma ray fluxes showing that the displacement seen in the top panel corresponds to a dip in the ratio with a minimum at the time of maximum of the gamma ray flux; bottom panel: calculations of the millimeter to gamma ray flux ratio, where the millimeter emission is produced by isotropic electrons in a uniform magnetic field viewed at 45° to the field direction.

the observed decay of the 80 GHz emission. The bremsstrahlung decays with about the same time constant, because the electron energy loss time in the thick target region is shorter than the time dependence of the electron source for this region, which is the precipitation, so that the decay is controlled by the same precipitation which controls the time behavior of the gyrosynchrotron radiation. As can be seen, for a given magnetic field, $F_{GS}(80GHz)/\Phi_B(>1MeV)$ decreases as the spectrum hardens. The observed delay of the bremsstrahlung relative to the gyrosynchrotron emission can thus be understood in terms of a hardening and subsequent softening of the accelerated electron spectrum, with the spectrum being hardest at the peak of the bremsstrahlung. The observed variation of the ratio from about 1000 to 250 thus implies a magnetic field of about 250 Gauss. A higher magnetic fields would follow from a recent analysis [27] which employed CGRO/OSSE data and found that the bremsstrahlung flux from the 1991 June 4 flare actually was lower by about a factor of 3 than that shown in Figure 1. The OSSE data, however, are still consistent with the BATSE/CPD time profile shown in Figure 1.

Gamma Ray Line Emission

Gamma ray lines were first observed from solar flares in 1972 with the NaI scintillator on OSO-7 [28]. But it was not until 1980 that routine observations became possible with the much more sensitive spectrometer on the Solar Maximum Mission (SMM [19,7]). Subsequently, gamma ray line observations were caried out with GRANAT/Phebus [29], CGRO [27], and YOHKOH [30]. Starting in 2000, observations with the imaging Ge spectrometer HESSI [31] should become available. Gamma-ray line emission in solar flares results from nuclear deexcitations, neutron capture and positron annihilation.

1 Deexcitation Lines: FIP, $(He/H)_{acc}$, $(He/H)_{amb}$, $(^3He/^4He)_{acc}$, $(Li/H)_{amb}$

Narrow deexcitation lines are produced by accelerated protons, α particles and ^{3}He nuclei interacting with ambient He and heavier nuclei, while broad lines result from interactions of accelerated C and heavier nuclei with ambient H and He. A theoretical nuclear deexcitation spectrum is shown in Figure 2. Starting from high energies, there are strong narrow lines at 6.13 MeV from ^{16}O, 4.44 MeV from ^{12}C, 1.79 MeV from ^{28}Si, 1.63 MeV from ^{20}Ne, 1.37 MeV from ^{24}Mg and 0.847 MeV from ^{56}Fe. All of these lines result from deexcitations in nuclei of the relatively abundant constituents of the solar atmosphere. This has allowed the determination of the abundances of these elements [32,9,33], showing that in the gamma ray production region the low FIP (first ionization potential) elements Mg, Si and Fe are enriched relative to C and O, a result which implies that the FIP bias, known to exist in the corona (e.g. [1]), already sets in at lower altitutes, presumably in the chromosphere.

Other important lines are formed in reactions between abundant constituents of both the accelerated particles and the ambient medium leading to excitations in nuclei which are otherwise rare in the solar atmosphere. The feature marked $\alpha\alpha$ is a blend of two lines, at 0.429 and 0.478 MeV from ^{7}Be and ^{7}Li, respectively. The excited states of these isotopes are populated by interactions of accelerated α particles with ambient He [34]. The line marked ^{3}He at 0.937 MeV and the narrow ^{59}Ni line at 0.339 MeV result, respectively, from interactions of accelerated ^{3}He nuclei with ambient ^{16}O and accelerated α particles with ^{56}Fe, leading to excited states in ^{18}F and ^{59}Ni [35]. The line complex marked (α,^{3}He) just above 1 MeV consists of 4 lines, at 1.04 and 1.08 MeV from the same ^{3}He induced reaction as that which produces the 0.937 MeV line, and at 1.00 and 1.05 MeV due to α particle interactions with ^{56}Fe leading to excited states in ^{58}Co, ^{58}Ni and ^{59}Ni. This complex was observed, but not resolved, with SMM [36,37]. We anticipate that with the Ge detectors on HESSI such resolution will be possible.

The various lines produced by accelerated α particles and ^{3}He nuclei provide information [38] on the He abundances in both the accelerated particles (the α/p ratio) and the ambient solar atmosphere, as well as the accelerated particle ^{3}He abundance (the ^{3}He/^{4}He ratio). In 5 flares out of 20 α/p was found to exceed the standard value of 0.1. The possibility of determining the accelerated α/p and its variation with time during the acceleration process from future more detailed gamma ray data will be an important ingredient for the understanding of solar flare particle acceleration [18]. In 4 flares out of 20 the ambient He abundance

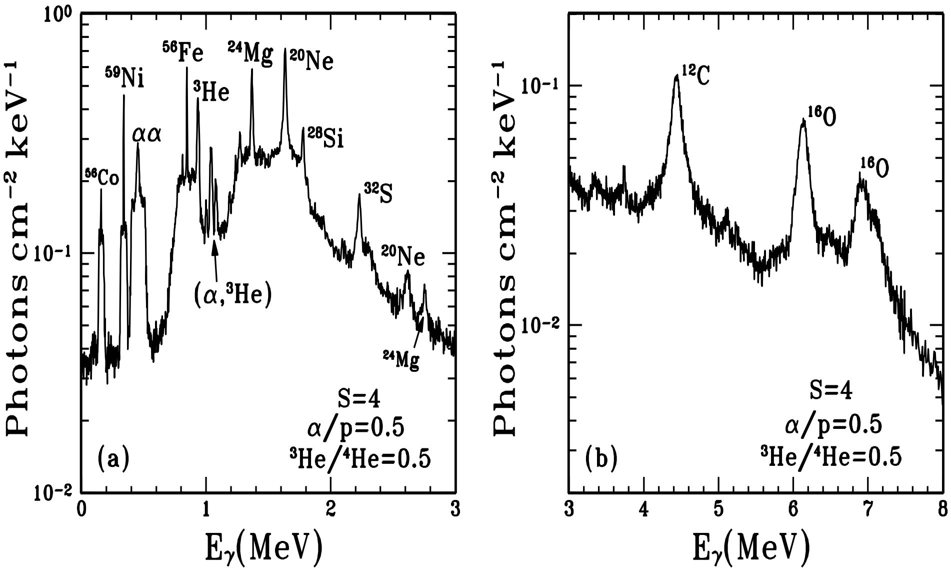

FIGURE 2. Theoretical nuclear deexcitation gamma-ray spectrum in two energy ranges. The accelerated particles energy spectrum is an unbroken power law with spectral index $S = 4$. Impulsive flare abundances are used for the accelerated particles, with α/p=0.5 and ^{3}He/^{4}He=0.5. The ambient medium abundances are those of the average corona, except that Ne/O=0.25.

was found to exceed its photospheric value (He/H=0.084 [39]), a result that has implications on solar atmospheric dynamics. Several flares required enhanced accelerated ^{3}He/^{4}He, meaning that the data definitely require the presence of ^{3}He induced reactions. For some of these flares, ^{3}He/^{4}He can be as high as 1, while for essentially all flares for which data are available, values of ^{3}He/^{4}He as large as 0.1 cannot be ruled out. As already mentioned, such ^{3}He/^{4}He enhancements are one of the main characteristics of the acceleration mechanism responsible for impulsive solar energetic particle events. One of the flares (1989 October 24), for which the evidence for enhanced ^{3}He/^{4}He is particularly strong, belongs to the class of gradual flares, based on the duration of the accompanying soft X-ray emission, showing that independent of the flare type, in both impulsive and gradual flares, the particles that interact and produce gamma rays are always accelerated by the same mechanism that operates in impulsive flares, namely stochastic acceleration through gyroresonant wave particle interaction (e.g. [18]).

The broad lines merge into the underlying emission upon which the narrow lines are superposed. By fitting theoretical gamma ray spectra to the total observed deexcitation spectra, it was shown [32,40] that the accelerated heavy ions, Ne, Mg, Si and Fe are enriched relative to C and O, an additional characteristic of impulsive flare acceleration. Very recently, individual broad lines have been resolved in a flare-averaged gamma-ray spectrum [41], and these also show heavy ion abundance enrichments, in particular for Fe.

The accelerated α particles also produce lithium, specifically via the reactions ^{4}He(α,p)^{7}Li, ^{4}He(α,n)^{7}Be$\rightarrow$^{7}Li and ^{4}He(α,pn)^{6}Li [42]. It was suggested [43] that such lithium production may account for the solar photospheric Li/H=1.4x10^{-11}. However, it was shown that this is not the case [44], even if the additional reaction ^{4}He(^{3}He,p)^{6}Li which becomes the dominant lithium production process for impulsive flare compositions and steep accelerated particle spectra, is included. In particular, based on all the available gamma ray line data and on the accelerated ion irradiation averaged over a solar cycle, the average Li production is about 2x10^{23} atoms/sec with about 80% of it being ^{6}Li [44]. Combined with the average solar wind flux of about 7.5x10^{35} protons/sec, and assuming that escape from the Sun in the solar wind is the dominant flare-produced Li removal preocess, one obtains Li/H=2.6x10^{-13} which is negligible in comparison with the photospheric Li/H. However, the calculated flare-produced ^{6}Li/H$\simeq$2.1x10^{-13} that escapes in the solar wind (again assuming this escape is the dominant removal process of the flare-produced Li) might account [45] for the recently measured solar wind Li isotopic ratio [46]. These measurements indicate ^{7}Li/^{6}Li = 31$\pm$4 in lunar soil, most likely due to solar wind implanted Li. Since the photospheric Li, mostly ^{7}Li, is depleted by over a factor of 100 relative to the protosolar ^{7}Li measured in meteorites, the much more fragile ^{6}Li should be depleted by a factor of about 10^6 (see [46]). This in turn means that in the solar wind the isotopic ratio ^{7}Li/^{6}Li of about 30 should result almost entirely from flare produced ^{6}Li. Combining the above given ^{6}Li/H due to flare production with the photospheric Li/H, we obtain a solar wind value of ^{7}Li/^{6}Li$\simeq$60. The factor of 2 difference between this and the measured value, is not significant given the uncertainties in the calculation. It is thus entirely possible that flare produced ^{6}Li was detected in the solar wind. The implications of this result are far reaching, as it can provide unique information on a variety of processes and parameters, including the mixing of flare produced isotopes in the solar atmosphere and the average accelerated particle irradiation of the Sun.

2 The Neutron Capture Line: Photospheric ^{3}He/H, Protosolar ^{2}H/H

The accelerated ions which produce the deexcitation lines also produce neutrons and positrons. The positrons annihilate directly or via positronium producing the 0.511 MeV line and the accompanying positronium continuum. These are not discussed in the present paper. A compilation of solar flare positron annihilation data can be found in [47]. For the theory of positron production and annihilation see [48,49].

The neutrons which propagate downward toward the photosphere are first thermalized and then captured on protons in the photosphere to produce deuterium and essentially monoenergetic photons at 2.223 MeV. This is the strongest line from flares, except for flares near the limb where it is strongly attenuated by Compton scattering of the line photons in the photosphere. In addition to captures on protons, a significant fraction of the neutrons in the photosphere are captured on photospheric ^{3}He nuclei [50]. The flux and time profile of the 2.223 MeV line thus depend on the photospheric ^{3}He abundance allowing the derivation of its abundance. Analysis of gamma ray data from the 1982 June 3 flare yielded ^{3}He/H=$(2.3{\pm}0.8){\times}10^{-5}$ or ^{3}He/H=$(1.8{\pm}0.8){\times}10^{-5}$, depending on the assumed angular distribution of the accelerated particles: tangential to the solar atmosphere or 4π isotropic, respectively [51]. Combining these values with the photospheric ^{4}He/H=0.084, we obtained [52] ^{3}He/^{4}He=$(2.7 \pm 0.9) \times 10^{-4}$ and ^{3}He/^{4}He=$(2.1 \pm 0.9) \times 10^{-4}$, for these two cases, respectively. These values can be compared with solar wind observations, ^{3}He/^{4}He $= (4.25 \pm 0.21) \times 10^{-4}$ [53], $(4.88 \pm 0.48) \times 10^{-4}$ [54] and $(4.4 \pm 0.4) \times 10^{-4}$ [55], obtained from Apollo, ISEE-3 and Ulysses data, respectively. We see that the photospheric ^{3}He/^{4}He is significantly lower than that of the solar wind. Since the FIPs of ^{3}He and ^{4}He are very close, this fractionation must be caused by the acceleration of solar wind, not matter transport from the photosphere to corona.

By taking the photospheric ^{3}He/^{4}He to be equal to average solar wind ratio, a model of solar evolution has been used to determine the protosolar deuterium abundance, $(^2\mathrm{H/H})_p = 2.675 \times 10^{-5} + (9.364 \times 10^{-2} - 2.452x)x$, where $x =^3$He/^{4}He - $4.0{\times}10^{-4}$, yielding $(^2\mathrm{H/H})_p = (3.01 \pm 0.17) \times 10^{-5}$ [56]. But by using the gamma ray data, specifically an average between the two values given above, we obtain a lower value, $(^2\mathrm{H/H})_p = (1.2 \pm 0.5) \times 10^{-5}$. Along with the present day deuterium abundance in the interstellar medium, $(^2\mathrm{H/H})_{ISM} = (1.47 - 1.72) \times 10^{-5}$ [57] and $(^2\mathrm{H/H})_{ISM} = (0.9 - 1.5) \times 10^{-5}$ [58], the protosolar deuterium provides the only other measurement for constraining the Galactic deuterium evolution, and thus the primordial ^{2}H/H (e.g. [59]). Our low protosolar ^{2}H/H provides an even stronger constraint on a high primordial deuterium abundance than the $(^2\mathrm{H/H})_p$ derived from the solar wind data (see [59]). Moreover, the almost equal protosolar and present day ISM deuterium abundance strengthens the need for the infall of primordial gas, that has recently received strong observational support [60].

REFERENCES

1. Reames, D. V., *Space Sci. Rev.*, **85**, 327 (1998).
2. Bastian, T. S., Benz, D. E., and Gary, D. E., *Annu. Rev. Astron. Astrophys.*, **36**, 131 (1998).
3. Kosugi, T., *High Energy Solar Physics*, eds. R. Ramaty, N. Mandzhavidze, and X.-M. Hua, (AIP: New York), 267 (1996).
4. Ramaty, R., and Mandzhavidze, N., *Highly Energetic Physical Processes and Mechanisms for Emission from Astrophysical Plasmas*, eds. P. C. H. Martens and S. Tsuruta, (IAU), in press.
5. Chupp, E. L. et al., *ApJ*, **318**, 913 (1987).
6. Ramaty, R., and Mandzhavidze, N., *Compton Gamma Ray Observatory*, eds. M. Friedlander et al. (New York: AIP), 643 (1993).
7. Chupp, E. L. *Physica Scripta*, **T18**, 15 (1990).
8. Lin, R. P., and Hudson, H. S., *Solar Physics*, **50**, 153 (1976).
9. Ramaty, R., Mandzhavidze N., Kozlovsky, B., and Murphy, R. J. 1995, *ApJ*, **445**, L193 (1995).
10. Share, G. H., and Murphy, R. J., *ApJ*, **452**, 933 (1995).
11. Cane, H. V., McGuire, R. E., and von Rosenvinge, T. T., *ApJ*, **301**, 448 (1986).
12. Bai, T., *ApJ*, **308**, 912 (1986).
13. Reames, D. V., *ApJ (Suppl.)*, **73**, 235 (1990).
14. Reames, D. V., Meyer, J-P., and von Rosenvinge, T. T., *ApJ (Suppl.)*, **90**, 649 (1994).
15. Kahler, S. W. *High Energy Solar Physics*, eds. R. Ramaty, N. Mandzhavidze, and X.-M. Hua, (AIP: New York), 61 (1996).
16. Lin, R. P. *Highly Energetic Physical Processes and Mechanisms for Emission from Astrophysical Plasmas*, eds. P. C. H. Martens and S. Tsuruta, (IAU), in press.
17. Miller, J. A. et al., *J. Geophys. Res.*, **102**, No. A7, 14,631 (1997).
18. Miller, J. A. 1998, *Space Sci. Rev.*, **86**, 79
19. Rieger, E., *Solar Physics*, **121**, 323 (1989).
20. Mandzhavidze, N., Ramaty, R., Bertsch, D. L., and Schneid, E. J., *High Energy Solar Physics*, eds. R. Ramaty, N. Mandzhavidze, and X.-M. Hua, (AIP: New York), 225 (1996).
21. Simnett, G. M., *Space Sci. Revs.*, **73**, 387 (1995).
22. Karlicky, M., Brown, J. C., Conway, A. J., and Penny, G. E., *A&A*, in press
23. Sakao, T. *PhD Thesis*, Natl. Astron. Obs., Tokyo, Japan (1994).
24. Ramaty, R., Schwartz, R. A., Enome, S., and Nakajima, N., *ApJ*, **436**, 941 (1994).

25. Ramaty, R., *Current Perspectives in High Energy Astrophysics*, ed. J. F. Ormes, (NASA Ref. Publ. 1391), 13 (1996).
26. Kaufmann, P., *High Energy Solar Physics*, eds. R. Ramaty, N. Mandzhavidze, and X.-M. Hua, (AIP: New York), 379 (1996).
27. Murphy, R. J. et al., *ApJ*, **490**, 883 (1997).
28. Chupp, E. L. et al., *Nature*, **241**, 333 (1973).
29. Barat, C. et al., *ApJ*, **425**, L109 (1994).
30. Yoshimori, M., *ApJ (Suppl.)*, **90**, 639 (1994)
31. Lin, R. P. et al., *SPIE*, **3442**, 2 (1998).
32. Murphy, R. J., Ramaty, R., Kozlovsky, B., and Reames, D. V. 1991, *ApJ*, **371**, 793 (1991)
33. Ramaty, R., Mandzhavidze N., and Kozlovsky, B., *High Energy Solar Physics*, eds. R. Ramaty, N. Mandzhavidze, and X.-M. Hua, (AIP: New York), 172 (1996).
34. Kozlovsky, B., and Ramaty, R., *ApJ*, **191**, L43 (1974).
35. Mandzhavidze, N., Ramaty, R., and Kozlovsky, B., *ApJ*, **489**, L99 (1997).
36. Murphy, R. J., Share, G. W., Letaw, J. R., and Forrest, D. J., *ApJ*, **358**, 298 (1990).
37. Share, G. H., and Murphy, R. J., *ApJ*, **508**, 876 (1998).
38. Mandzhavidze, N., Ramaty, R., and Kozlovsky, B., *ApJ*, **518**, 918 (1999).
39. Richard, O. et al., *A&A*, **338**, 756 (1998).
40. Ramaty, R., Mandzhavidze, N., Barat, C., & Trottet, G. 1997, *ApJ*, **479**, 458 (1997).
41. Share, G. H., and Murphy, R. J., *26th Internat. Cosmic Ray Conf.*, (Salt Lake City), **6**, 13 (1999).
42. Ramaty, R., Kozlovsky, B., Lingenfelter, R., and Reeves, H., *ApJ*, **488**, 730 (1997).
43. Kotov, Yu., D., Bogovalov, S. V., Endalova, O. V., and Yoshimori, M., *ApJ*, **473**, 514 (1996).
44. Mandzhavidze, N., Ramaty, R., and Kozlovsky, B., *25th Internat. Cosmic Ray Conference*, (Durban), **1**, 9 (1997).
45. Tatischeff, V., Thibaud, J. P., and Ramaty, R, in preparation (2000).
46. Chaussidon, M., and Robert, F., *Nature*, **402**, 270 (1999).
47. Vestrand, W. T. et al., *ApJ (Suppl.)*, **120**, 409 (1999).
48. Kozlovsky, B., Lingenfelter, R. E., and Ramaty, R., *ApJ*, **316**, 801 (1987).
49. Guessoum, N., Ramaty, R., and Lingenfelter, R. E., *ApJ*, **378**, 170 (1991).
50. Wang, H. T., and Ramaty, R., *Solar Physics*, **36**, 129 (1974).
51. Hua, X.-M., and Lingenfelter, R. E., *ApJ*, **319**, 555 (1987).
52. Mandzhavidze, N., and Ramaty, R., *Highlights of Astronomy*, ed. J. Andersen (IAU), **11B**, 759 (1998).
53. Geiss, J. et al., *Appolo Prelim. Science Report*, NASA SP-315, sec. 14 (1972).
54. Coplan, M. A. et al., *Solar Physics*, **128**, 195 (1990).
55. Bodmer, R. et al., *Space Sci. Rev.*, **72**, 61 (1994).
56. Gautier, D., and Morel, P., *A&A*, **323**, L9 (1997).
57. Linsky, J. L. et al., *ApJ*, **402**, 694 (1993).
58. Lemoine, M. et al., *A&A*, **308**, 601 (1996).
59. Tosi, M., Steigman, G., Matteucci, and Chiappini, C., *ApJ*, **498**, 226 (1998).
60. Wakker, B. P. et al., *Nature*, **402**, 388 (1999).